R. & M. No. 3163
(19,292)
A.R.C. Technical Report

MINISTRY OF AVIATION

AERONAUTICAL RESEARCH COUNCIL
REPORTS AND MEMORANDA

Measurements of the Direct Hinge-Moment Derivatives at Subsonic and Transonic Speeds for a Cropped Delta Wing with Oscillating Flap

By

J. B. BRATT, B.A., B.Sc., C. J. W. MILES and R. F. JOHNSON,
of the Aerodynamics Division, N.P.L.

LONDON: HER MAJESTY'S STATIONERY OFFICE
1960
EIGHT SHILLINGS NET

Measurements of the Direct Hinge-Moment Derivatives at Subsonic and Transonic Speeds for a Cropped Delta Wing with Oscillating Flap

By

J. B. BRATT, B.A., B.Sc., C. J. W. MILES and R. F. JOHNSON,
of the Aerodynamics Division, N.P.L.

Reports and Memoranda No. 3163*
May, 1957

Summary.—Measurements of the direct hinge-moment derivatives at subsonic and transonic speeds have been made for a cropped delta wing of aspect ratio 1·8 with an oscillating full-span flap. The measurements were obtained with new derivative apparatus fitted to the National Physical Laboratory $9\frac{1}{2}$-in. High Speed Tunnel, and some account is given of the estimation of apparatus errors.

The effect of amplitude of oscillation ξ_0 and frequency parameter ω on the derivatives has been investigated; a maximum value for ω of 0·25 at $M = 1 \cdot 0$ being attained.

A comparison of the measured derivatives with theory shows satisfactory agreement for the damping and reasonable agreement for the stiffness at subsonic speeds. At supersonic speeds ($M = 1 \cdot 1$) large discrepancies occur.

1. *Introduction.*—The measurements of direct flap derivatives described in this paper were made with the new derivative apparatus designed for the N.P.L. $9\frac{1}{2}$-in. High Speed Tunnel, and they form the first reliable results obtained with this equipment. Since there are 18 derivatives to be measured for the wing-flap combination under test, and for each derivative 5 parameters to be varied, namely, Mach number, frequency of oscillation, amplitude of oscillation, wing incidence and flap setting, the programme becomes long-term in nature. In view of this it was decided to divide the work into separate parts, selected in the first instance to bring out in succession the teething troubles in the three main parts of the equipment, namely, the two vibrating systems and the force unit (frame plus force pick-ups). This has the merit of giving some useful results without first ensuring that the whole of the equipment is working satisfactorily and at the same time enables suggested improvements to be put in hand for incorporation at a later date when a different part of the apparatus is in use.

The general arrangement of the apparatus is shown in Figs. 1 and 2, which are taken from an earlier report[1] describing the experimental technique. For the present tests the exciter coils were connected to the smaller vibrating system, and the wing was clamped to the frame in a position enabling the tongue on the flap to mate with that on the neighbouring steel cylinder. The frame was clamped to earth since the force pick-ups were not required in this instance.

When the system was vibrating the node was situated near the drive end of the torsion bar at a distance varying from 1/5 to 1/9 of its length, depending on frequency. This position resulted from design considerations in which the inertia at the model end of the system was reduced to a minimum consistent with rigidity in order to attain the highest frequency for a given torsion bar stiffness.

* Published with the permission of the Director, National Physical Laboratory.

Measurements of h_ξ and $h_{\dot{\xi}}$ have been obtained with both wing and flap set at zero incidence, and with amplitudes of oscillation ξ_0 of 1 deg and 2 deg. The tunnel was fitted with slotted liners to enable continuous variation of Mach number through the speed of sound to be obtained. For each amplitude the Mach number ranged from 0·4 to 1·1 and the frequency parameter ω from 0·07 to 0·25 at $M = 1 \cdot 0$. The frequency range covered was from 27 c.p.s. to 104 c.p.s.

As far as the authors are aware a self-excited system oscillating in a free-free mode has not previously been employed for derivative measurements. The advantage gained is avoidance of power dissipation in the fixed structure due to the latter taking up large reactions from the tuning spring. However, this advantage is obtained at the expense of greater complication in the estimation of the stiffness derivative and the apparatus damping corrections. These points are discussed in Section 5 and in more detail in the Appendices.

2. *Details of Model.*—The model under test was a cropped delta wing with full-span trailing-edge flap hinged at its leading edge and is illustrated in Fig. 3. This particular plan-form was chosen for comparison with theoretical work by Garner[2], whilst at the same time it is reasonably representative of certain present-day trends. The data given below relate to a complete wing.

Aspect ratio	1·8
Taper ratio	0·143
Flap/mean chord ratio	25 per cent
Thickness/chord ratio	6 per cent
Section	RAE 102
Apex angle	61·92 deg
Sweepback (Leading edge)	59·04 deg
Sweepback (Trailing edge)	0 deg
Span	8·228 in.
Root chord	8·000 in.
Tip chord	1·143 in.
Mean chord	4·572 in.
Flap chord	1·143 in.

The model is constructed of solid steel, the flap being hinged to the wing by means of a flat steel strip 0·002 in. thick clamped to both wing and flap in the mid plane of the wing section and extending the whole length of the span to form a sealed gap. For simplicity in construction this gap was given the form of a straight cut perpendicular to the chord and 0·02 in. wide.

3. *Experimental Results.*—Values of h_ξ were derived from measurements of the change in natural frequency of the dynamic system due to the addition of the aerodynamic stiffness forces. These frequency changes amounted to approximately 10 per cent with the weakest torsion bar and highest Mach number ($f = 27$ c.p.s., $M = 1 \cdot 026$) and 0·14 per cent with the stiffest torsion bar and lowest Mach number ($f = 104$ c.p.s., $M = 0 \cdot 4$). The inherent accuracy in measuring the very small frequency change of the latter case was within 2 per cent since the uncertainty in the measurement of a frequency with the electronic-counter equipment employed was one part in 10^5. A calibration of the dynamic system giving frequency change as a function of added stiffness was obtained by adding known inertias to the model end of the system and calculating the equivalent stiffness from the relation $H_\xi = p^2 \delta I$. From three such measurements the coefficients in a formula relating frequency change to added stiffness could be obtained (*see* Appendix III).

The damping derivative coefficient $h_{\dot{\xi}}$ was obtained from the difference between measurements of the electrical power input to the exciter coils for the same amplitude of oscillation with the tunnel running and in still air. This power difference ranged from approximately 2 milliwatts up to $0 \cdot 4$ watts. All power measurements were corrected for ohmic, eddy current and magnetic hysteresis loss, which amounted in total to approximately 6 per cent for the lowest and 35 per cent for the highest powers.

Still-air power was roughly 30 per cent of the total power at the lowest Mach number ($M = 0 \cdot 4$) and 10 per cent of the total at the Mach number giving maximum damping ($M = 0 \cdot 97$). These rather large values of apparatus damping appear to be inherent in apparatus designed for measurement at high Mach numbers and the higher values of frequency parameter when an oscillating system tuned by a spring is employed. There is some evidence to suggest that an upper limit to the frequency parameter exists above which reliable measurements could not be obtained with this technique on account of the apparatus damping swamping the aerodynamic damping.

Curves showing the variation of $-h_{\dot{\xi}}$, $-h_{\xi}$ and ω with Mach number for given still-air frequencies ranging from 27 to 104 c.p.s. are shown in Figs. 4 to 11. The damping derivative $-h_{\dot{\xi}}$ shows a slow rise from $M = 0 \cdot 4$ to between $0 \cdot 7$ and $0 \cdot 8$, after which a more rapid rise sets in leading to a peak value at approximately $M = 0 \cdot 97$. Following the peak a very rapid fall occurs leading to a region of negative damping between $M = 1 \cdot 02$ and $1 \cdot 12$. The negative experimental points near the limits of this region were obtained by adjusting the Mach number to give a sustained oscillation with no drive and equating the aerodynamic damping to the apparatus damping. It was found impossible to obtain measurements by the normal method within the negative region on account of violent fluctuations in the meter readings due presumably to unsteadiness in the flow over the flap.

The stiffness derivative h_{ξ} rises very slightly from $M = 0 \cdot 4$ to $0 \cdot 9$, after which a very rapid rise sets in which persists into the negative damping region. The presence of a peak in this region is indicated by a falling branch of the curve on the high-Mach-number side.

Effects of amplitude of oscillation are shown by measurements at amplitudes of 1 deg and 2 deg. In the case of the damping derivative the difference is negligible. The stiffness derivative shows a small but definite effect, the 1-deg curve lying slightly below that for 2 deg between $M = 0 \cdot 4$ and $1 \cdot 0$, the greatest difference occurring where the curve begins to rise rapidly.

The influence of frequency parameter is shown in Fig. 12, which was obtained by cross-plotting the curves for 2-deg amplitude discussed above. At the lower Mach numbers the damping derivative falls slightly with increasing ω, but on approaching the peak value a rising curve is obtained. The stiffness derivative shows an increase with ω for all Mach numbers in the range plotted.

Cross-plots for higher values of Mach number were not attempted in view of the rapid change of damping and stiffness with M.

In connection with the damping curves (Figs. 4 to 7) the question arises as to whether the sudden fall in damping could be associated in any way with tunnel resonance effects[3]. With solid liners the Mach number at which resonance would be expected ranges from $0 \cdot 999$ to $0 \cdot 976$ as the frequency varies from 27 to 104 c.p.s. (based on the diagonal of the working-section). As far as can be observed there is no corresponding trend in the curves of Figs. 4 to 7, which suggests that resonance effects are not significant. This is supported by American rocket tests on an uncropped delta with flap which showed a similar sudden loss of damping. The effect of slotted liners on tunnel resonance is not known.

4. *Comparison with Theory*.—Subsonic theoretical values for $M = 0$ and $0 \cdot 7454$, which are valid for very small values of the frequency parameter have been obtained by Garner[2] using an extension of the Multhopp-Garner theory, and points are included in Figs. 4 to 11 and 13. The damping derivative $h_{\dot{\xi}}$ shows satisfactory agreement with experiment, whereas the stiffness points indicate a theoretical curve rising more steeply than experiment and reaching a value 50 per cent higher at $M = 0 \cdot 7454$. This discrepancy is thought to be due to viscous effects, which in general have a greater influence on stiffness than on damping forces.

Supersonic theoretical curves obtained by Watson[4] are included in Figs. 4 to 7 for $h_{\dot{\xi}}$ and in Fig. 13 for both $h_{\dot{\xi}}$ and h_{ξ}. These curves relate to a frequency parameter tending to zero, the effect of which is small according to theory over the range of the experiments. Considerable divergence between experiment and theory is evident over the range of supersonic Mach numbers covered, the theoretical damping recovering from negative values at a much higher Mach number and the stiffness showing a much delayed fall compared with experiment.

An overall picture of the comparison with theory is given in Fig. 13.

5. *Corrections to Measurements.*—The influence of the following factors on the measurements of h_{ξ} and $h_{\dot{\xi}}$ was investigated, and where the effect was found to be appreciable a correction was applied. A more detailed analysis relating to Sub-sections 5.4 and 5.5 is given in the Appendices.

5.1. *Leakage of Air into Apparatus Box.*—The vibratory system is contained in a box fixed to the wall of the tunnel and communicating with the working-section *via* an aperture in the tunnel wall through which the tongue of the model passes. An air-leak in the box gives rise to flow into the tunnel at the root of the model when the pressure in the working-section falls on running the tunnel.

Although no pressure difference between working-section and box had been detected, a leak of this nature was discovered on attempting to evacuate the box (sealed off at the tunnel end) to determine the corrections discussed in 5.2. From measurements of the rate of leak it was estimated that the average normal velocity of inflow into the tunnel reached a maximum of the order of 10 per cent of the tunnel velocity in the region of $M = 1$. Some difficulty was experienced in sealing this leak, and finally a reduction of inflow velocity from 10 per cent to 1 per cent was taken as acceptable. A large number of the derivative measurements were repeated, and from these corrections to the earlier measurements were determined. These corrections amounted to 2 or 3 per cent on both damping and stiffness at the lower Mach numbers, and about 6 per cent on the peak damping and 20 per cent on stiffness at $M = 1$ where the curve is rising very steeply.

5.2. *Air Density in Apparatus Box.*—For each wind-on condition measurements of the still-air power and frequency were made at atmospheric pressure, and the changes relative to these datum values due to the wind were used in calculating the derivatives. Strictly, the power datum should be obtained with the pressure in the apparatus box equal to its value with the tunnel running and with zero still-air damping on the model. The frequency datum should relate to the same pressure condition, but in this case should include the still-air virtual inertia on the model as well as on moving parts in the box since the stiffness derivative corresponds to the difference between aerodynamic forces in the wind and in still air.

In order to determine the errors introduced by using the atmospheric datum values, a cover box was fitted over the model to seal the system completely, and measurements of power and frequency were made with the system evacuated to various values of pressure. The change in still-air power for complete evacuation of the system varied from less than 1 per cent up to 2 per cent over the frequency range (27 c.p.s. to 104 c.p.s.), and the change in frequency from 0·13 per cent to 0·025 per cent. Corrections based on these measurements were negligible in the case of the damping and ranged around − 1 per cent for the stiffness. A constant correction of − 1 per cent was applied in the latter case.

5.3. *Change in Temperature of Oscillating System.*—In view of the very small frequency changes involved in the measurement of h_{ξ} when using the stiffest torsion bar, the effect of change in temperature on the still-air natural frequency of the system due to running the tunnel was estimated from measurements of the temperature change in the apparatus box made with the aid of a thermo-couple. At the lower Mach numbers, where the effect is most important, the temperature difference between wind-on and mean still-air conditions amounted to not more than 0·05 deg C. This gives an error in the stiffness derivative of less than 0·5 per cent when used in conjunction with a temperature coefficient on frequency of 0·0125 per cent per deg C derived from known values of the coefficient of expansion and the temperature coefficient of the rigidity modulus for the steels used in the construction of the equipment. No correction was applied for this effect.

5.4. *Effect of Mode on Apparatus Damping.*—The vibratory system performs a free-free oscillation in which the model end and drive end are very nearly 180 deg out of phase. The effect of the wind forces is to change the amplitude of the drive end, the phase angle between the ends, and the frequency of oscillation; thus the apparatus damping with the wind on differs from that in still air. Since the still-air power was used in correcting the total power for apparatus damping, some error was introduced, and the magnitude of this is discussed briefly below and in more detail in Appendix II.

An analysis of power relations in the system leads to an expression for the apparatus damping power containing six terms, two relating to air damping in the apparatus box, three to hysteresis damping in springs, and one to air damping on the driving coil assembly outside the box. In view of the test results quoted in Section 5.2 the first two terms may be ignored and consideration given to the relative magnitudes of the remaining four. An expression is obtained in Appendix IV for the phase angle (difference from 180 deg) between the two ends of the system in still air based on the assumption that damping terms other than the term representing power dissipation in the torsion bar (including its end clamps) are negligible. A calculated value of 0·575 deg for the weakest torsion bar agrees well with a measured value of 0·56 deg obtained optically with an auto-stroboscope arrangement and leads to the conclusion that the still-air damping resides mainly in the torsion bar. Phase-angle measurements for the stiffer torsion bars were less reliable on account of the smaller values, but from general considerations the torsion-bar damping term would be expected to increase more rapidly than the other three terms with increasing stiffness, and the conclusion relating to the distribution of damping remains valid.

It follows from the above conclusion and from Appendix II that the still-air damping power may be written in the form

$$\frac{P'}{\xi_0^2} = \bar{H}_2 p'(r' + 1)^2 \qquad \ldots \quad \ldots \quad \ldots \quad \ldots \quad \ldots \qquad (1)$$

for the small phase angles arising in the tests. The effect on the derivatives of changing p and r to the values obtained in the wind-on measurements was calculated and found to be not more than $\frac{1}{2}$ per cent in the worst case. This error has been ignored. The amplitude ratio r was derived from measurements of the back E.M.F. in the driving coils and a datum still-air value obtained optically.

A more satisfactory method of examining the distribution of still-air damping which will be tried in future tests, would be to determine each of the four damping terms from a set of four equations each relating to a different mode of vibration (amplitude ratio and frequency) obtained by changing an inertia.

5.5. *Effect of Mode on Stiffness Measurements.*—The stiffness derivatives were calculated from the formula

$$-H_\xi = c\,\frac{1 - a\Delta}{1 - b\Delta}\,\Delta\,, \quad \ldots \quad \ldots \quad \ldots \quad \ldots \quad \ldots \quad \ldots \qquad (2)$$

where $\Delta = p^2 - p'^2$, and a, b, c were regarded as constants. These were determined by simulating three different values of H_ξ by changing the inertia at the model end of the system ($H_\xi = p^2 \delta I$) and solving the set of equations given by (2). It follows from the analysis in Appendix III that the coefficients a, c are constant only for a system with zero damping, and that in general they are functions of amplitude ratio, phase angle and driving power. Since the effect of change in air density was examined experimentally (Section 5.2), the analysis was limited to the case of constant air density for simplicity and led to expressions for c and a proportional to Y and $1/Y$ respectively, where

$$Y = E + FX' + G\frac{X - X'}{\Delta}, \quad \ldots \quad \ldots \quad \ldots \quad \ldots \qquad (3)$$

E, F and G being constants for the system, and X, X' functions of driving power, phase angle and amplitude ratio.

The variation in Y over the range of conditions arising both in the stiffness derivative measurements and the inertial calibration was calculated from (3) and was found to be less than $0 \cdot 1$ per cent in the worst case. The assumption regarding the constancy of a and c is thus seen to be valid to a degree well within the accuracy of the measurements.

Values for the phase angles ε and ε' required in (3) were calculated by the method given in Appendix IV based on the assumption that all the apparatus damping is in the torsion bar.

6. *Conclusions.*—The main conclusions of this report are as follows :

(1) The damping derivative $-h_{\dot{\xi}}$ rises rapidly above $M = 0 \cdot 8$ to a peak value at $M = 0 \cdot 97$. A rapid fall follows the peak leading to a region of negative damping between $M = 1 \cdot 02$ and $1 \cdot 12$.

(2) The stiffness derivative $-h_{\xi}$ shows a very steep rise above $M = 0 \cdot 9$ which continues through $M = 1 \cdot 0$ and is followed by a rapid fall.

(3) Both the damping and stiffness derivatives increase with frequency parameter ω at the higher subsonic values of Mach number. At the lower Mach numbers the stiffness still increases with ω, whilst the damping shows a small decrease.

(4) At subsonic Mach numbers agreement with theory is satisfactory for the damping. The theoretical stiffness rises more steeply than indicated by experiment to a value 50 per cent higher at $M = 0 \cdot 75$. At supersonic Mach numbers both the recovery of damping from negative values and the fall in the value of the stiffness following its steep rise occur much earlier than predicted by supersonic theory.

(5) Experience with the present apparatus suggests that with derivative apparatus employing a spring tuned system the ratio of apparatus damping to aerodynamic damping at a given Mach number increases as the maximum frequency parameter at which the apparatus is designed to make measurements is increased. This suggests that an upper limit to the frequency parameter exists above which reliable measurements could not be obtained with this technique.

7. *Acknowledgement.*—Assistance in the experimental work and in the analysis of results was given by Mrs. N. C. Woodgate of the Aerodynamics Division, N.P.L.

LIST OF SYMBOLS

a, b, c		Coefficients in equation (2) for H_ξ in Section 5.5
$\bar{c}_f$		Mean chord of flap
$\bar{c}$		Mean chord of wing and flap combination
E, F, G		Constants in equation (III.12)
f		Frequency of oscillation
h_ξ	=	$H_\xi/\rho V^2 S_f \bar{c}_f$
$h_{\dot\xi}$	=	$H_{\dot\xi}/\rho V S_f \bar{c}\bar{c}_f$
H_ξ		Direct hinge-moment stiffness coefficient
$H_{\dot\xi}$		Direct hinge-moment damping coefficient
H		Flap hinge moment $= H_\xi \xi + H_{\dot\xi}\dot\xi$
H_1, H_2, H_3		Hysteresis power loss in springs (*see* Fig. 14)
$\bar{H}_1, \bar{H}_2, \bar{H}_3$		Non-dimensional form of H_1 H_2, H_3 (*see* equation (II.9))
I_1, I_2		Inertias in vibratory system (*see* Fig. 14)
M_θ		Direct pitching-moment stiffness coefficient
$M_{\dot\theta}$		Direct pitching-moment damping coefficient
M		Mach number
M_1		Driving moment
$\bar{M}_1$		Non-dimensional form of driving moment (*see* equation (I.5))
p		Circular frequency $= 2\pi f$
P		Total driving power
P_a		Wind damping power
P_1, P_2		Still-air damping power at drive and model ends (*see* Fig. 14)
$\bar{P}_1, \bar{P}_2, \bar{P}_c$		Non-dimensional forms of P_1, P_2 (*see* equation (II.9))
r		Amplitude ratio $= -\bar{\theta}_1/\bar{\theta}_2$
S_f		Area of flap
t		Time
T		Back reaction on driving spindle due to twist of torsion bar
V		Wind speed
X		Function defined by equation (III.5)
Y		Function defined by equation (III.11)
Δ	=	$p^2 - p'^2$
ε		Phase angle between motions of drive end and model spindles
$\varepsilon_1, \varepsilon_2, \varepsilon_3$		Phase angles associated with complex elastic stiffnesses (*see* Fig. 14)
θ_1, θ_2		Displacements of drive and model spindles (*see* Fig. 14)
$\bar{\theta}_1, \bar{\theta}_2$		Amplitudes of θ_1 and θ_2
K_1, K_2		Still-air damping coefficients for drive and model ends of system
ξ		Flap displacement
ξ_0		Amplitude of flap displacement
ρ		Air density
σ		Function defined by equation (III.4)
$\sigma_1, \sigma_2, \sigma_3$		Complex spring stiffnesses (*see* equation (I.4) and Fig. 14)
$\bar{\sigma}_1, \bar{\sigma}_2, \bar{\sigma}_3$		Amplitudes of σ_1, σ_2, σ_3
ω		Frequency parameter $= p\bar{c}/V$

Dashed symbols relate to still-air conditions.

REFERENCES

No.	Author	Title, etc.
1	J. B. Bratt	A note on derivative apparatus for the N.P.L. $9\frac{1}{2}$-in. High Speed Tunnel. C.P.269. January, 1956.
2	H. C. Garner	Application of Multhopp's lifting-surface theory to the lift, pitching moment and hinge moment on a slowly pitching cropped delta wing with oscillating flap. (To be published.)
3	D. S. Woolston and H. L. Runyan	Some considerations on the air forces on a wing oscillating between two walls for subsonic compressible flow. *J.Ae.Sci.* Vol. 22. No. 1. p. 41. January, 1955.
4	J. Watson	Calculation of derivatives for a cropped delta wing with an oscillating constant-chord flap in a supersonic air stream. R. & M. 3059. November, 1955.

APPENDIX I

Equations of Motion of Vibratory System

The essential features of the system are shown diagrammatically in Fig. 14, displacements of the spindles being indicated by θ_1 and θ_2. For the drive end

$$I_1\ddot{\theta}_1 + K_1\dot{\theta}_1 + (\sigma_1 + \sigma_2)\theta_1 = M_1 + \sigma_2\theta_2 \,, \qquad \text{(I.1)}$$

where K_1 is still-air damping and M_1 is the moment applied by the vibrators.

For the model end

$$I_2\ddot{\theta}_2 + (K_2 - M_{\dot{\theta}})\dot{\theta}_2 + (\sigma_2 + \sigma_3 - M_\theta)\theta_2 = \sigma_2\theta_1 \,, \qquad \text{(I.2)}$$

where K_2 is still-air damping and M_θ, $M_{\dot{\theta}}$ relate to the aerodynamic moment about the axis due to the wind. Aerodynamic acceleration terms are included in the structural inertias.

A solution of the form

$$\theta_2 = \bar{\theta}_2 \, e^{jpt}, \quad \theta_1 = \bar{\theta}_1 \, e^{j(pt+\varepsilon} \qquad \text{(I.3)}$$

is assumed, and hysteresis effects in springs are represented by the introduction of the complex elastic stiffnesses

$$\sigma_1 = \bar{\sigma}_1 \, e^{j\varepsilon_1} \,, \quad \sigma_2 = \bar{\sigma}_2 \, e^{j\varepsilon_2} \,, \quad \sigma_3 = \bar{\sigma}_3 \, e^{j\varepsilon_3} \,. \qquad \text{(I.4)}$$

In practice the driving moment is adjusted to be in quadrature with the displacement of the model and may thus be given the form

$$M_1 = j\bar{M}_1\theta_2 \, e^{jpt} \,, \qquad \text{(I.5)}$$

where $\bar{M}_1$ is constant.

Substitution in (I.1) and (I.2) leads to the following four equations :

$$(\bar{\sigma}_1 \cos \varepsilon_1 + \bar{\sigma}_2 \cos \varepsilon_2 - p^2 I_1)\bar{\theta}_1 = \{\bar{M}_1 \sin \varepsilon + \bar{\sigma}_2 \cos (\varepsilon_2 - \varepsilon)\}\bar{\theta}_2 \,, \qquad \text{(I.6)}$$

$$(\bar{\sigma}_1 \sin \varepsilon_1 + \bar{\sigma}_2 \sin \varepsilon_2 + pK_1)\bar{\theta}_1 = \{\bar{M}_1 \cos \varepsilon + \bar{\sigma}_2 \sin (\varepsilon_2 - \varepsilon)\}\bar{\theta}_2 \,, \qquad \text{(I.7)}$$

$$\bar{\sigma}_2 \cos (\varepsilon_2 + \varepsilon) \,.\, \bar{\theta}_1 = (\bar{\sigma}_2 \cos \varepsilon_2 + \bar{\sigma}_3 \cos \varepsilon_3 - M_\theta - p^2 I_2)\bar{\theta}_2 \,, \qquad \text{(I.8)}$$

$$\bar{\sigma}_2 \sin (\varepsilon_2 + \varepsilon) \,.\, \bar{\theta}_1 = \{\bar{\sigma}_2 \sin \varepsilon_2 + \bar{\sigma}_3 \sin \varepsilon_3 + p(K_2 - M_{\dot{\theta}})\}\bar{\theta}_2 \,. \qquad \text{(I.9)}$$

The solution of these equations gives the two modes of vibration of the system, one with a node between the spindles and the other with an external node. In the tests the first of these modes is excited, and for this case both $\bar{\theta}_1/\bar{\theta}_2$ and $\bar{M}_1$ are negative and ε is small.

APPENDIX II

Power Relations

The expressions tabulated below relate to the power dissipated in the various parts of the vibratory system.

Driving power $= P = f\oint M_1\, d\theta_1 = \frac{1}{2}p\bar{M}_1\bar{\theta}_1\bar{\theta}_2 \cos \varepsilon$ . .. . (II.1)

Hysteresis loss :

Spring 1 $= H_1 = f\oint \sigma_1\theta_1\, d\theta_1 = \frac{1}{2}p\bar{\sigma}_1\bar{\theta}_1{}^2 \sin \varepsilon_1$, ... (II.2)

Spring 2 $= H_2 = f\oint \sigma_2(\theta_1 - \theta_2)\, d(\theta_1 - \theta_2) = \frac{1}{2}p\bar{\sigma}_2(\bar{\theta}_1{}^2 - 2\bar{\theta}_1\bar{\theta}_2 \cos \varepsilon + \bar{\theta}_2{}^2)$, (II.3)

Spring 3 $= H_3 = f\oint \sigma_3\theta_2\, d\theta_2 = \frac{1}{2}p\bar{\sigma}_3\bar{\theta}_2{}^2 \sin \varepsilon_3$ . .. . (II.4)

Still air damping :

Drive-end loss $= P_1 = f\oint K_1\dot{\theta}_1\, d\theta_1 = \frac{1}{2}K_1p^2\bar{\theta}_1{}^2$, ... (II.5)

Model-end loss $= P_2 = f\oint K_2\dot{\theta}_2\, d\theta_2 = \frac{1}{2}K_2p^2\bar{\theta}_2{}^2$, ... (II.6)

Wind damping $= P_a = -f\oint M_{\dot{\theta}}\dot{\theta}_2\, d\theta_2 = -\frac{1}{2}M_{\dot{\theta}}p^2\bar{\theta}_2{}^2$ . .. . (II.7)

Substitution of the above expressions in (I.7) and (I.9) leads to

$$P = P_a + P_1 + P_2 + H_1 + H_2 + H_3 , \qquad \text{(II.8)}$$

which simply expresses the fact that the driving power is equal to the total power dissipated.

The quantity measured in a test may now be expressed in the form

$$\frac{P}{\bar{\theta}_2{}^2} = \frac{P_a}{\bar{\theta}_2{}^2} + \bar{P}_1\rho p^2r^2 + \bar{P}_c p^2r^2 + \bar{P}_2\rho p^2 + \bar{H}_1pr^2$$
$$+ \bar{H}_2p(r^2 + 2r\cos\varepsilon + 1) + \bar{H}_3p , \qquad \text{(II.9)}$$

where $\bar{P}$, $\bar{H}$, etc., are constants and $r = -\bar{\theta}_1/\bar{\theta}_2$. The still-air damping in the apparatus box is assumed to be proportional to ρ, and K_1 has been split into two parts (coefficients $\bar{P}_1$ and $\bar{P}_c$), one of which represents the air damping on the driving coils, for which ρ is constant.

In view of the considerations discussed in Section 5.2, the apparatus damping relating to flap oscillation may thus be written

$$\frac{P'}{\xi_0{}^2} = \bar{P}_c p'^2r'^2 + \bar{H}_1p'r'^2 + \bar{H}_2p'(r'^2 + 2r'\cos\varepsilon' + 1) + \bar{H}_3p' \qquad \text{(II.10)}$$

by neglecting the terms involving ρ. The further considerations of Section 5.4, indicating that the apparatus damping is practically wholly contained in the torsion bar, are expressed by retaining the third term only on the right-hand side of (II.10) ; for small phase angles this leads to

$$\frac{P'}{\xi_0{}^2} = \bar{H}_2p'(r' + 1)^2 . \qquad \text{(II.11)}$$

The damping derivative for flap oscillation was calculated from the formula

$$-\tfrac{1}{2}H_{\dot{\xi}}p^2\xi_0{}^2 = P - P' \qquad \text{(II.12)}$$

and the effect of errors in P' examined in the manner described in Section 5.4.

APPENDIX III

Aerodynamic Stiffness Formulae

It is assumed in the following analysis that the air density in the apparatus box and tunnel working-section is the same for still air as with the tunnel running. The effect of the change in density which occurs on running the tunnel has been discussed in Section 5.2 in relation to the flap measurements given in this report.

Equation (I.8) leads to

$$-M_\theta = (p^2 - p'^2)I_2 + \bar{\sigma}_2\{r \cos(\varepsilon_2 + \varepsilon) - r' \cos(\varepsilon_2 + \varepsilon')\}, \quad \text{(III.1)}$$

which on elimination of r and r' with the aid of (I.6) gives

$$-M_\theta = I_2\Delta + \bar{\sigma}_2\left(\frac{X}{\sigma - I_1\Delta} - \frac{X'}{\sigma}\right), \quad \text{(III.2)}$$

where

$$\Delta = p^2 - p'^2, \quad \text{(III.3)}$$

$$\sigma = \bar{\sigma}_1 \cos\varepsilon_1 + \bar{\sigma}_2 \cos\varepsilon_2 - p'^2 I_1, \quad \text{(III.4)}$$

$$X = \{\bar{M}_1 \sin\varepsilon + \bar{\sigma}_2 \cos(\varepsilon_2 - \varepsilon)\}\cos(\varepsilon_2 + \varepsilon), \quad \text{(III.5)}$$

$$X' = \{\bar{M}_1' \sin\varepsilon' + \bar{\sigma}_2 \cos(\varepsilon_2 - \varepsilon')\}\cos(\varepsilon_2 + \varepsilon'). \quad \text{(III.6)}$$

The expression (III.2) may be rewritten in the more convenient form

$$-M_\theta = c\frac{1 - a\Delta}{1 - b\Delta}\Delta, \quad \text{(III.7)}$$

where

$$a = \frac{I_1 I_2 \sigma}{Y}, \quad \text{(III.8)}$$

$$b = \frac{I_1}{\sigma}, \quad \text{(III.9)}$$

$$c = \frac{Y}{\sigma^2}, \quad \text{(III.10)}$$

and

$$Y = I_2\sigma^2 + I_1\bar{\sigma}_2 X' + \frac{\bar{\sigma}_2\sigma(X - X')}{\Delta}, \quad \text{(III.11)}$$

$$= E + FX' + G\frac{X - X'}{\Delta}, \quad \text{(III.12)}$$

where E, F, G are constants. Values for $\bar{M}_1$, $\bar{M}_1'$ in X, X' may be obtained from (II.1) in the form

$$\bar{M}_1 = -\frac{P}{\bar{\theta}_2^{\,2}}\frac{2}{pr\cos\varepsilon} \quad \text{(III.13)}$$

and the phase angles calculated by the method given in Appendix IV.

In the theoretical case of zero internal and external damping the driving power and phase angles vanish to give constant and equal values to X and X'. Thus Y and hence the coefficients in (III.7) are constant.

The stiffness derivative for flap oscillation was calculated from the formula

$$-H_\xi = c\frac{1 - a\Delta}{1 - b\Delta}\Delta, \quad \text{(III.14)}$$

where a, b, c were assumed to be constants. The validity of this procedure is discussed in Section 5.5.

APPENDIX IV

Calculation of Phase Angles

From (I.3) and (I.4) it follows that the back reaction T on the driving spindle due to twist of the torsion bar is given by the expression

$$T = \{\bar{\theta}_1 e^{j(pt+\varepsilon)} - \bar{\theta}_2 e^{jpt}\}\bar{\sigma}_2 e^{j\varepsilon_2}. \qquad \text{(IV.1)}$$

If it is now assumed that work is done only *via* the torsion bar, the driving power may be expressed in the form

$$P = f\oint T\, d\theta_1 = f\bar{\sigma}_2 \oint \{\bar{\theta}_1 \sin(pt + \varepsilon + \varepsilon_2) - \bar{\theta}_2 \sin(pt + \varepsilon_2)\}\, d\theta_1\,, \qquad \text{(IV.2)}$$

where $\theta_1 = \bar{\theta}_1 \sin(pt + \varepsilon)$. This leads to the relation

$$\frac{P}{\bar{\theta}_2^{\,2}} = \pi f \bar{\sigma}_2 r\{\sin(\varepsilon_2 - \varepsilon) + r \sin \varepsilon_2\}\,, \qquad \text{(IV.3)}$$

$$= \pi f \bar{\sigma}_2 r\{(r + 1)\varepsilon_2 - \varepsilon\} \qquad \text{(IV.4)}$$

for small angles.

The value of ε_2 may be obtained by considering oscillation in still air if in this case it is assumed that all the work done is in the torsion bar including its end clamps. For this condition the moment T' exerted by the torsion bar on the spindle at the model end of the system will be in phase with the motion of the spindle. Thus from (I.3) and (IV.1)

$$r' \sin(\varepsilon' + \varepsilon_2) + \sin \varepsilon_2 = 0\,, \qquad \text{(IV.5)}$$

which for small angles gives

$$r'\varepsilon' + (r' + 1)\varepsilon_2 = 0\,. \qquad \text{(IV.6)}$$

Expressions for the phase angles in terms of driving power, frequency, amplitude ratio and torsion bar stiffness may be now derived from (IV.4) and (IV.6) in the form

$$\pi\bar{\sigma}_2\varepsilon = \frac{r + 1}{f'(r' + 1)^2} \cdot \frac{P'}{\bar{\theta}_2^{\,2}} - \frac{1}{fr} \cdot \frac{P}{\bar{\theta}_2^{\,2}}\,, \qquad \text{(IV.7)}$$

$$\pi\bar{\sigma}_2\varepsilon' = -\frac{1}{f'r'(r' + 1)}\,\frac{P'}{\bar{\theta}_2^{\,2}}\,, \qquad \text{(IV.8)}$$

$$\pi\bar{\sigma}_2\varepsilon_2 = \frac{1}{f'(r' + 1)^2} \cdot \frac{P'}{\bar{\theta}_2^{\,2}}\,. \qquad \text{(IV.9)}$$

TABLE 1

Values of $-h_{\dot{\xi}}$ *and* $-h_{\xi}$

f'	Test	M	ξ_0	ω	$-h_{\dot{\xi}}$	$-h_{\xi}$	ξ_0	ω	$-h_{\dot{\xi}}$	$-h_{\xi}$
27 c.p.s.	1	0·397	1·94°	0·1523	+0·210	0·261	0·975°	0·1522	0·202	0·251
	2	0·397	1·95	0·1515	0·219	0·261	0·975	0·1525	0·200	0·253
	3	0·397	1·95	0·1520	0·207	0·260				
	4	0·498	1·94	0·1223	0·224	0·255	0·970	0·1233	0·220	0·250
	5	0·498					0·975	0·1230	0·221	0·251
	6	0·597	1·94	0·1042	0·241	0·268	0·965	0·1048	0·240	0·254
	7	0·597	1·94	0·1044	0·242	0·259	0·970	0·1044	0·233	0·255
	8	0·597					0·970	0·1046	0·236	0·254
	9	0·597					0·975	0·1043	0·233	0·257
	10	0·597					0:970	0·1045	0·236	0·257
	11	0·695	1·95	0·0911	0·260	0·272	0·970	0·0914	0·250	0·266
	12	0·695	1·95	0·0910	0·255	0·271	0·970	0·0915	0·251	0·265
	13	0·695					0·960	0·0906	0·256	0·265
	14	0·795	1·94	0·0813	0·281	0·282	0·965	0·0817	0·277	0·274
	15	0·795	1·94	0·0810	0·280	0·281	0·970	0·0814	0·276	0·273
	16	0·896	1·94	0·0734	0·374	0·291	0·970	0·0737	0·358	0·278
	17	0·896	1·94	0·0735	0·375	0·289	0·970	0·0736	0·356	0·278
	18	0·896					0·970	0·0739	0·375	0·283
	19	0·920	1·95	0·0716	0·421	0·298	0·970	0·0721	0·407	0·283
	20	0·946	1·93	0·0704	0·471	0·336	0·975	0·0704	0·492	0·308
	21	0·946	1·93	0·0710	0·480	0·330	0·970	0·0705	0·475	0·302
	22	0·946					0·960	0·0704	0·514	0·309
	23	0·958	1·95	0·0700	0·493	0·366				
	24	0·958	1·94	0·0705	0·512	0·358				
	25	0·958	1·94	0·0697	0·479	0·370				
	26	0·969	1·95	0·0696	0·504	0·408	0·975	0·0697	0·522	0·381
	27	0·969	1·94	0·0701	0·530	0·405	0·965	0·0695	0·546	0·368
	28	0·969	1·94	0·0701	0·509	0·409				
	29	0·969	1·93	0·0695	0·492	0·371				
	30	0·982	1·94	0·0696	0·460	0·476				
	31	0·982	1·95	0·0698	0·495	0·474				
	32	0·982	1·95	0·0693	0·485	0·493				
	33	0·994	1·94	0·0693	0·406	0·593	0·975	0·0698	0·389	0·584
	34	0·994					0·970	0·0698	0·379	0·583
	35	1·006	1·94	0·0702	0·240	0·738	0·975	0·0706	0·125	0·747
	36	1·018	1·93	0·0709	+0·014	0·990				
	37	{1·019	1·95	0·0713	−0·060	1·069				
	38	{1·077	1·95	0·0679	−0·060	0·776				
53	39	0·397	2·01	0·2915	+0·197	0·276	1·000	0·2925	0·197	0·270
	40	0·597	2·01	0·1985	0·236	0·267				
	41	0·695					1·000	0·1739	0·260	0·270
	42	0·795	2·01	0·1538	0·289	0·286				
	43	0·896	1·99	0·1398	0·371	0·293	1·000	0·1395	0·376	0·282
	44	0·946	2·01	0·1329	0·463	0·362				
	45	0·969	1·99	0·1312	0·508	0·446	1·000	0·1315	0·560	0·411
	46	0·982	1·99	0·1317	0·451	0·534				
	47	1·006	1·99	0·1291	+0·191	0·775	1·000	0·1298	0·240	0·768
	48	{1·019	2·01	0·1289	−0·039	0·946				
	49	{1·094	2·01	0·1219	−0·040	0·749				
	50	1·117	2·00	0·1195	−0·009	0·734	1·000	0·1210	0·040	0·718

Brackets indicate limits of negative damping region.

TABLE 1—*continued*

f'	Test	M	ξ_0	ω	$-h_{\dot{\xi}}$	$-h_{\xi}$	ξ_0	ω	$-h_{\dot{\xi}}$	$-h_{\xi}$
79 c.p.s.	51	0·397	1·98°	0·4396	+0·194	0·286	0·980°	0·4381	0·188	0·279
	52	0·597	1·98	0·3000	0·231	0·288				
	53	0·695					0·985	0·2600	0·253	0·287
	54	0·795	1·97	0·2332	0·304	0·301				
	55	0·896	1·97	0·2092	0·410	0·308	0·980	0·2082	0·401	0·297
	56	0·946	1·97	0·2002	0·513	0·362				
	57	0·969	1·97	0·1966	0·537	0·447	0·975	0·1956	0·547	0·412
	58	0·982	1·97	0·1948	0·523	0·548				
	59	1·006	1·97	0·1929	+0·221	0·792	0·980	0·1919	0·263	0·791
	60	1·021	1·96	0·1903	−0·039	0·995				
	61	1·094	1·96	0·1808	−0·039	0·894				
	62	1·117	1·97	0·1766	+0·006	0·769	0·980	0·1769	0·033	0·746
104	63	0·397	1·94	0·5760	0·188	0·296	0·985	0·5814	0·198	0·292
	64	0·397	1·94	0·5821	0·193	0·293				
	65	0·498	1·94	0·4650	0·206	0·293				
	66	0·597	1·94	0·3875	0·227	0·297				
	67	0·597	1·96	0·3916	0·226	0·299				
	68	0·695	1·94	0·3408	0·254	0·307	0·990	0·3459	0·263	0·283
	69	0·746	1·95	0·3219	0·263	0·306				
	70	0·746	1·94	0·3263	0·275	0·306				
	71	0·746	1·96	0·3191	0·275	0·309				
	72	0·795	1·95	0·3031	0·302	0·313				
	73	0·795	1·96	0·3021	0·307	0·314				
	74	0·844	1·95	0·2939	0·331	0·315				
	75	0·844	1·96	0·2876	0·334	0·321				
	76	0·896	1·95	0·2732	0·402	0·326	0·985	0·2764	0·397	0·309
	77	0·920	1·95	0·2697	0·442	0·331				
	78	0·920	1·95	0·2688	0·450	0·341				
	79	0·946	1·96	0·2607	0·489	0·391	0·995	0·2630	0·549	0·311
	80	0·946	1·96	0·2605	0·514	0·381				
	81	0·958	1·95	0·2584	0·546	0·427				
	82	0·969	1·95	0·2568	0·540	0·481	0·985	0·2587	0·570	0·437
	83	0·969	1·95	0·2560	0·558	0·412				
	84	0·982	1·97	0·2569	0·549	0·565				
	85	0·994	1·95	0·2519	0·415	0·669	0·990	0·2538	0·509	0·598
	86	1·006	1·98	0·2535	+0·258	0·773	0·990	0·2519	0·268	0·780
	87	1·027	1·98	0·2506	−0·062	1·058				
	88	1·092	1·98	0·2381	−0·063	0·795				
	89	1·036	1·98	0·2469	−0·060	1·088				
	90	1·102	1·98	0·2353	−0·061	0·893				
	91	1·117	1·97	0·2339	0·001	0·790	0·991	0·2335	0·028	0·766

Brackets indicate limits of negative damping region.

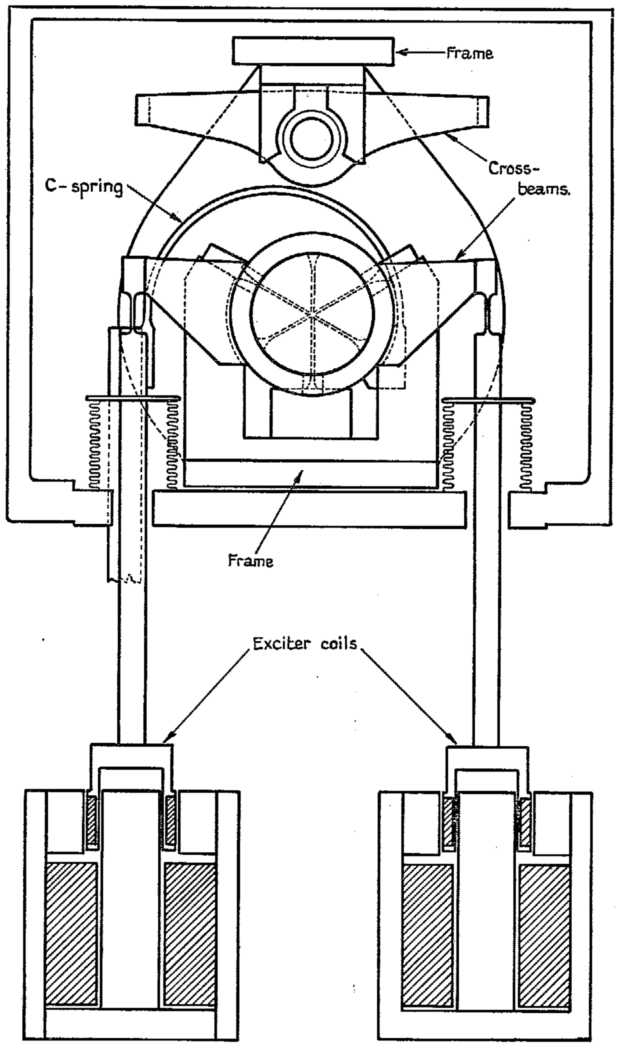

FIG. 1. General arrangement of apparatus. End view.

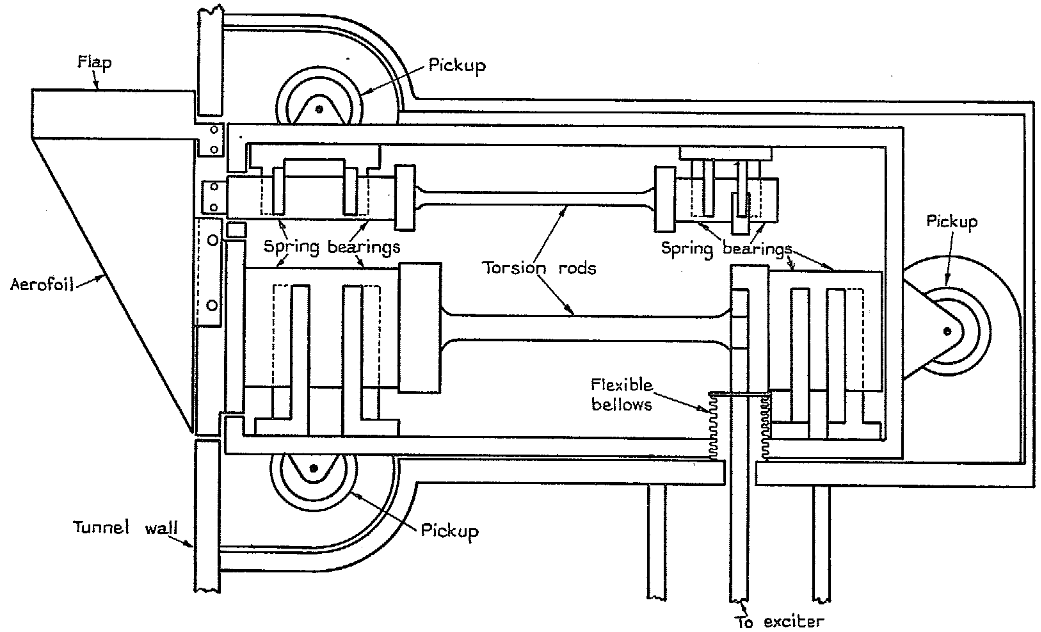

FIG. 2. General arrangement of apparatus. Side view.

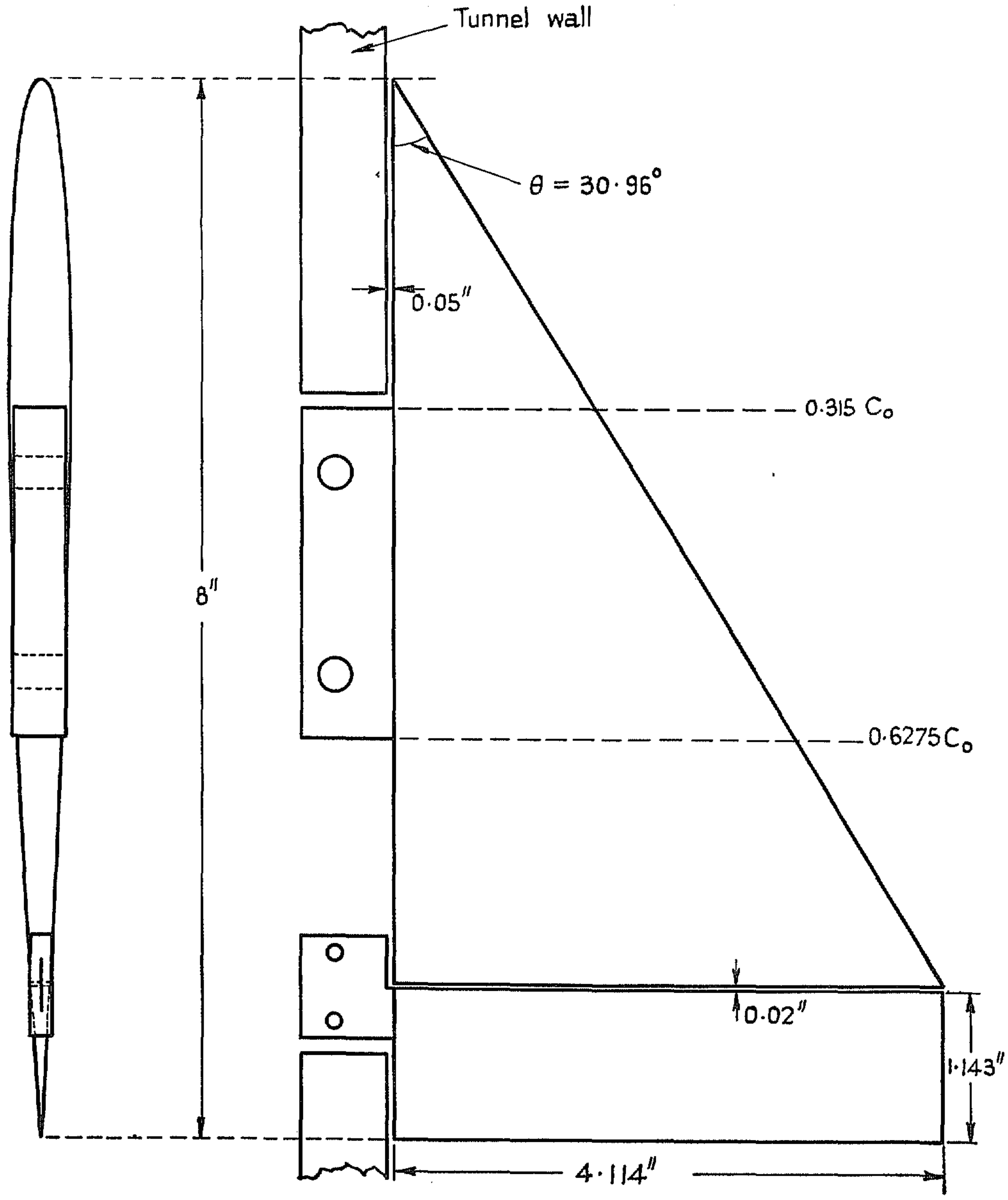

FIG. 3. Diagram of model.

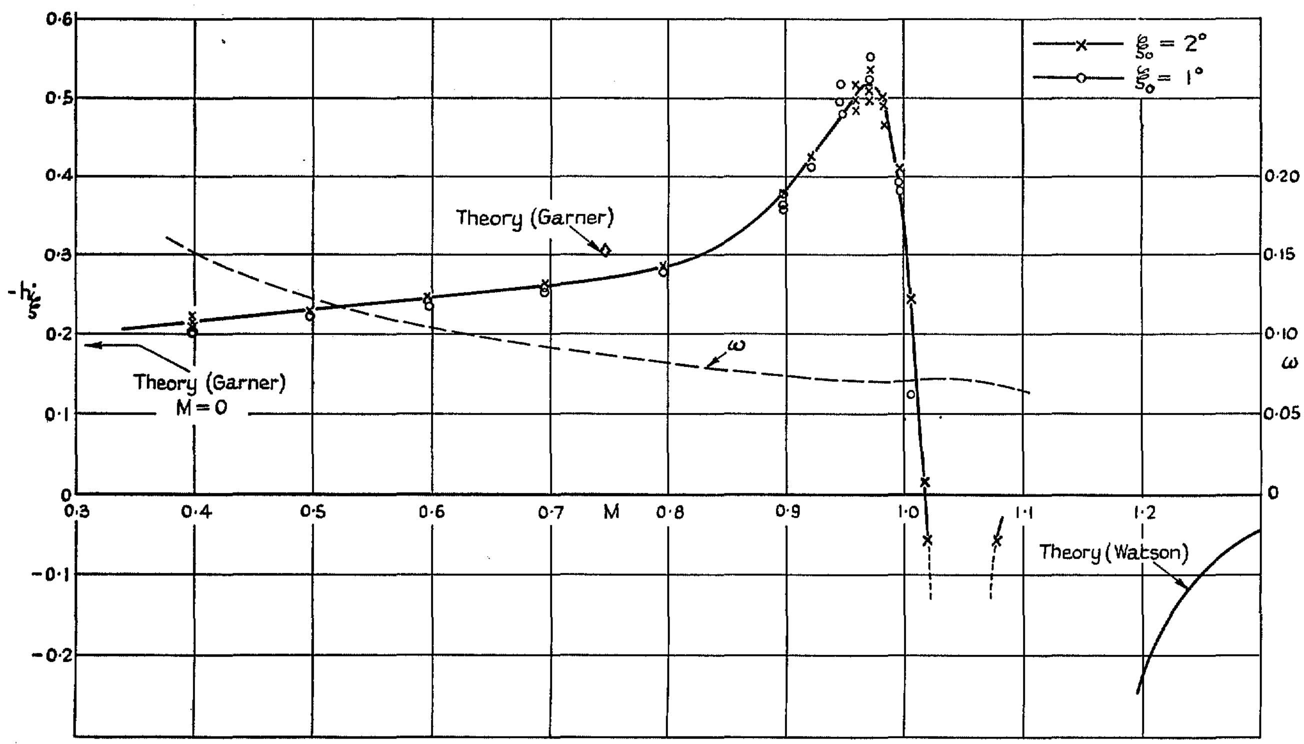

FIG. 4. Variation of $-h_{\dot{\xi}}$ and ω with M for $f' = 27$ c.p.s.

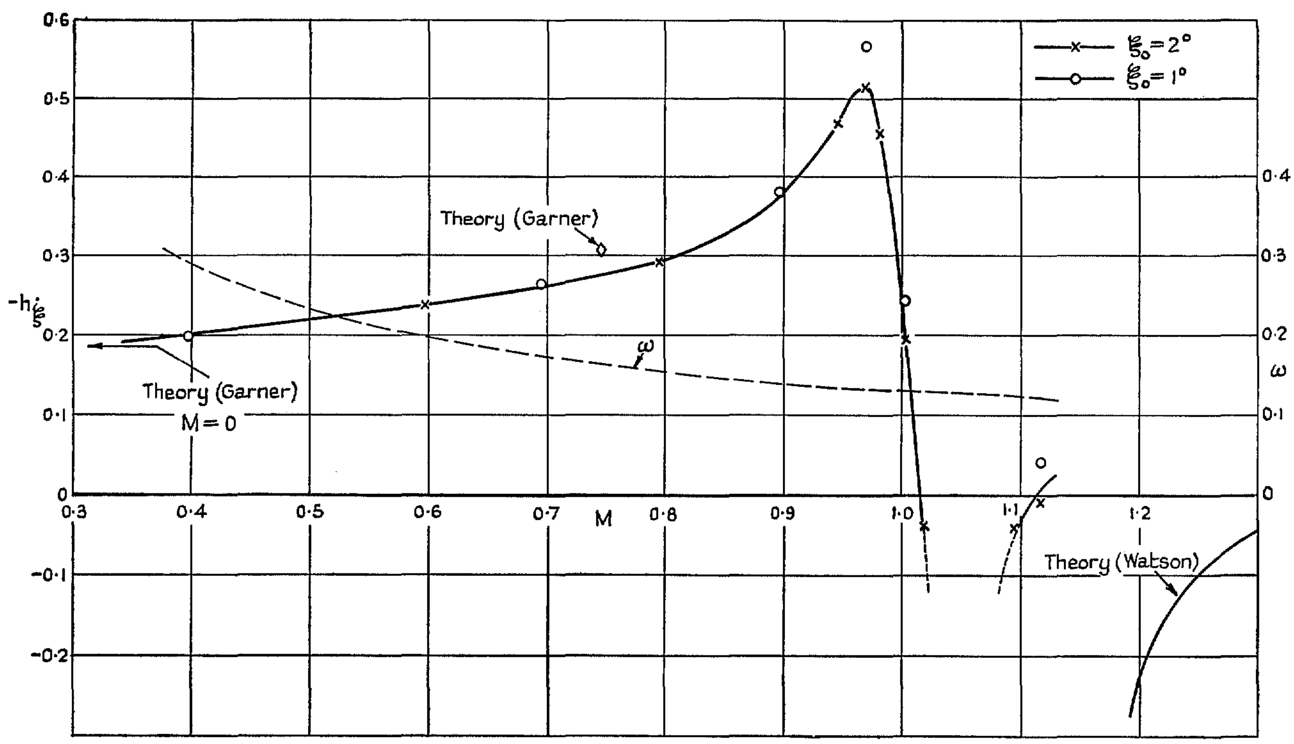

FIG. 5. Variation of $-h_{\dot{\xi}}$ and ω with M for $f' = 53$ c.p.s.

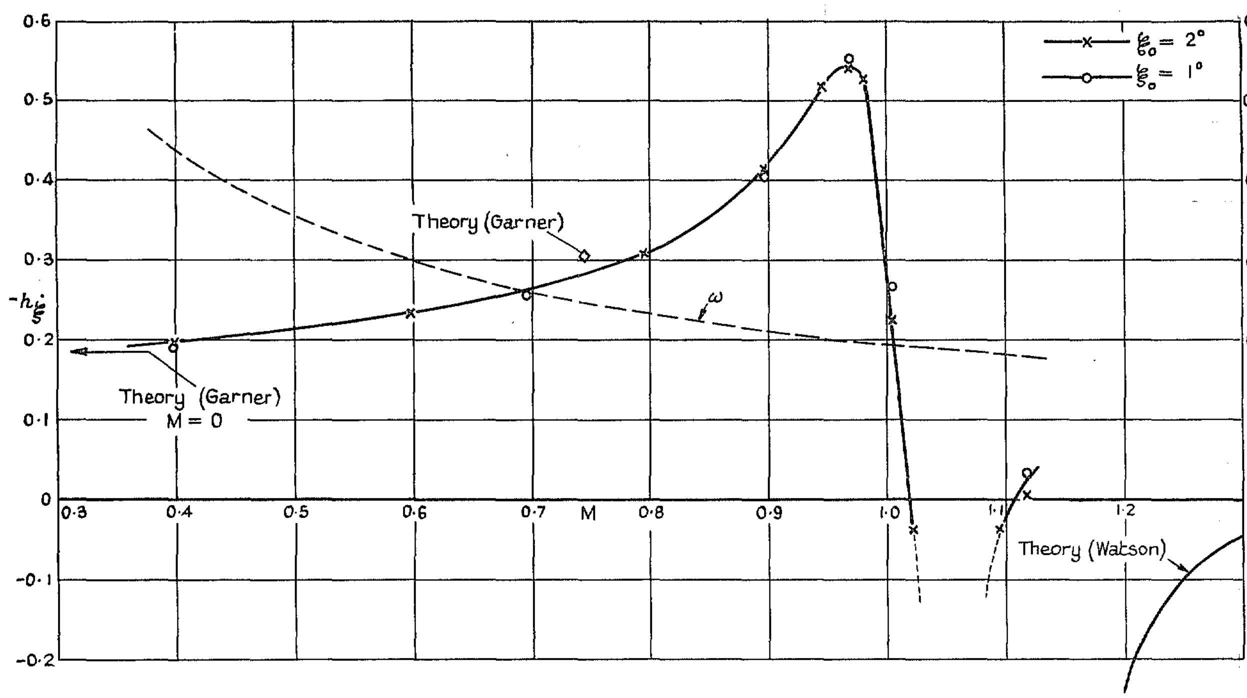

FIG. 6. Variation of $-h_{\dot{\xi}}$ and ω with M for $f' = 79$ c.p.s.

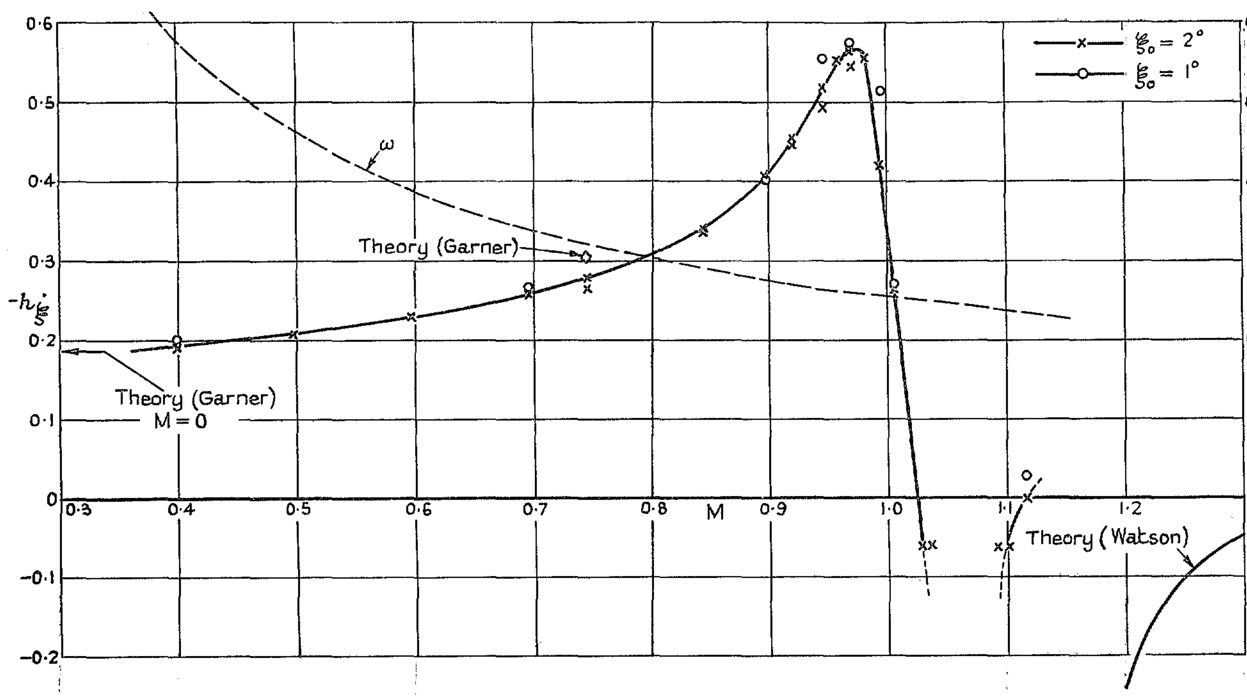

FIG. 7. Variation of $-h_{\dot{\xi}}$ and ω with M for $f' = 104$ c.p.s.

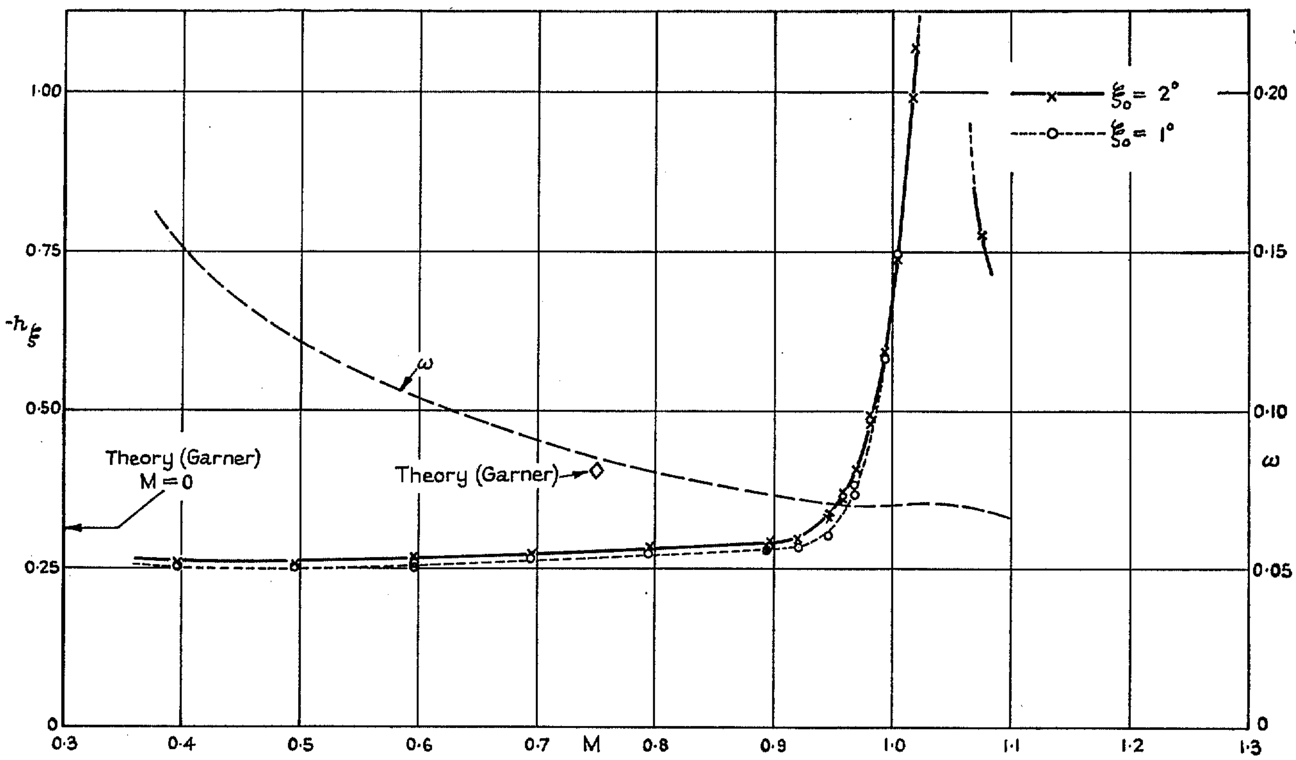

FIG. 8. Variation of $-h_\xi$ and ω with M for $f' = 27$ c.p.s.

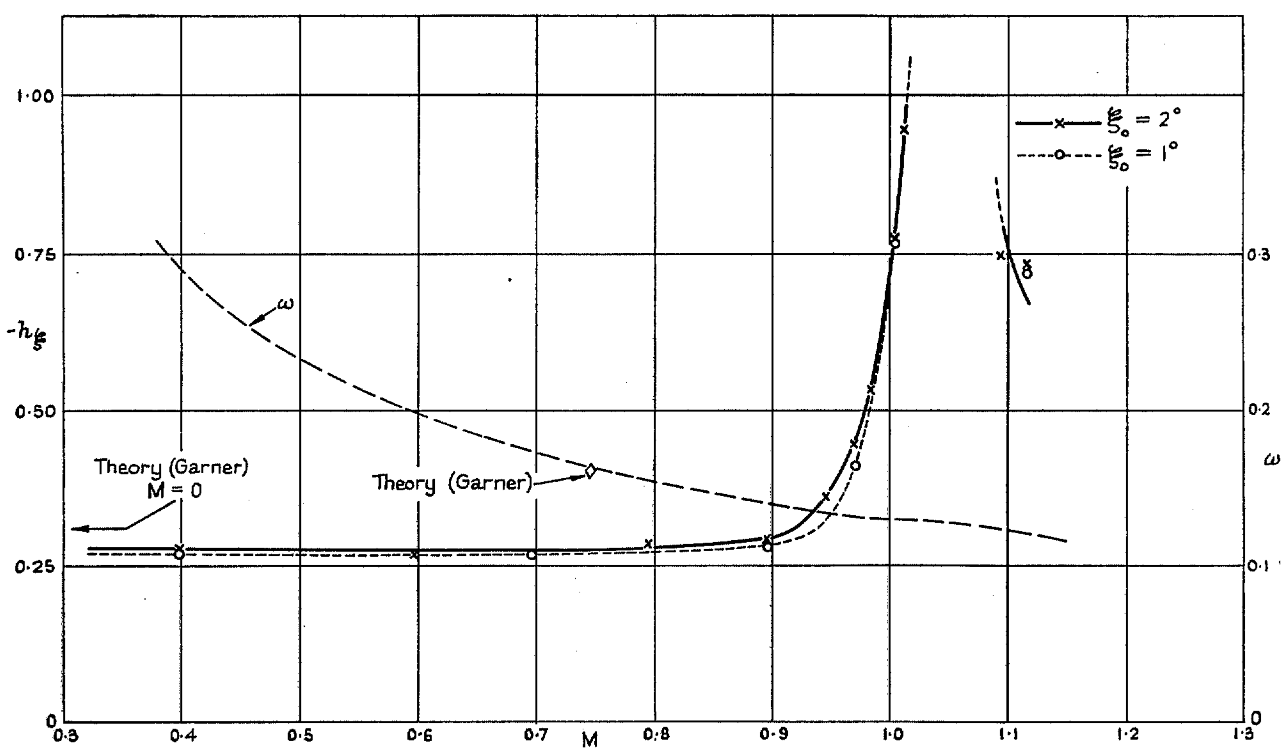

FIG. 9. Variation of $-h_\xi$ and ω with M for $f' = 53$ c.p.s.

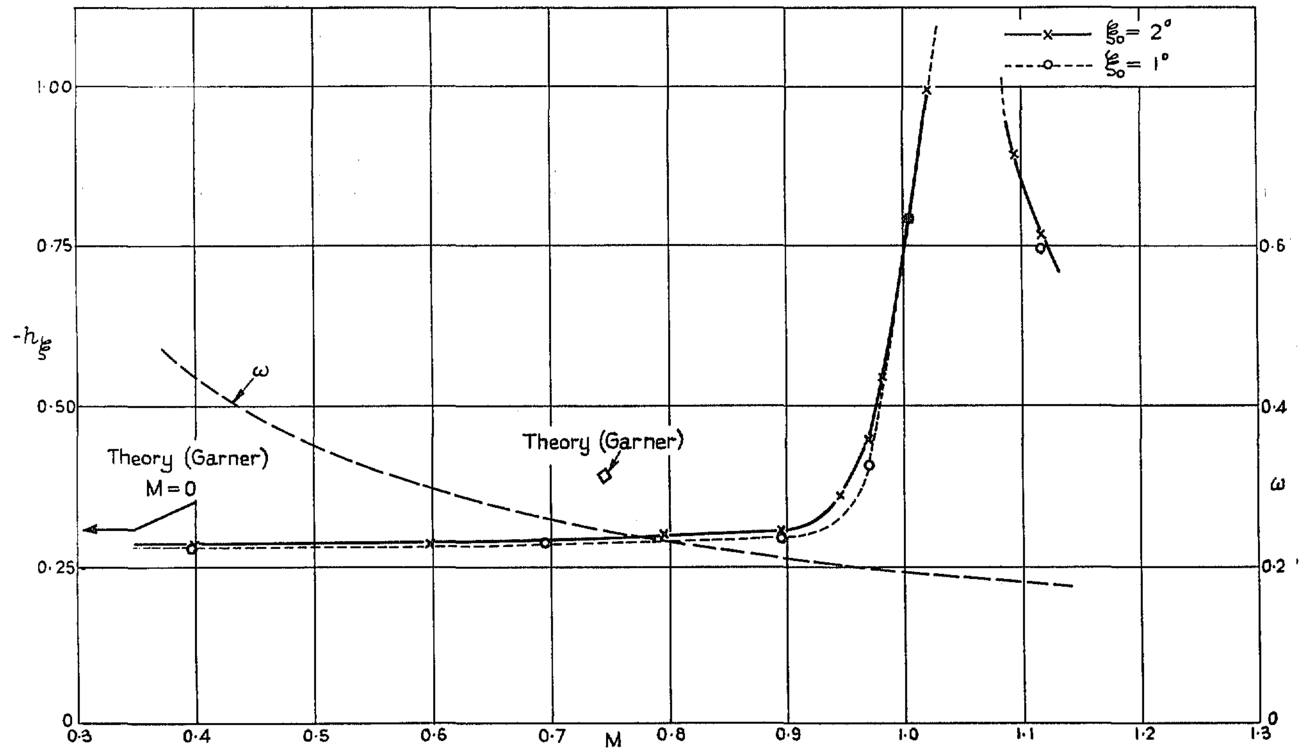

FIG. 10. Variation of $-h_\xi$ and ω with M for $f' = 79$ c.p.s.

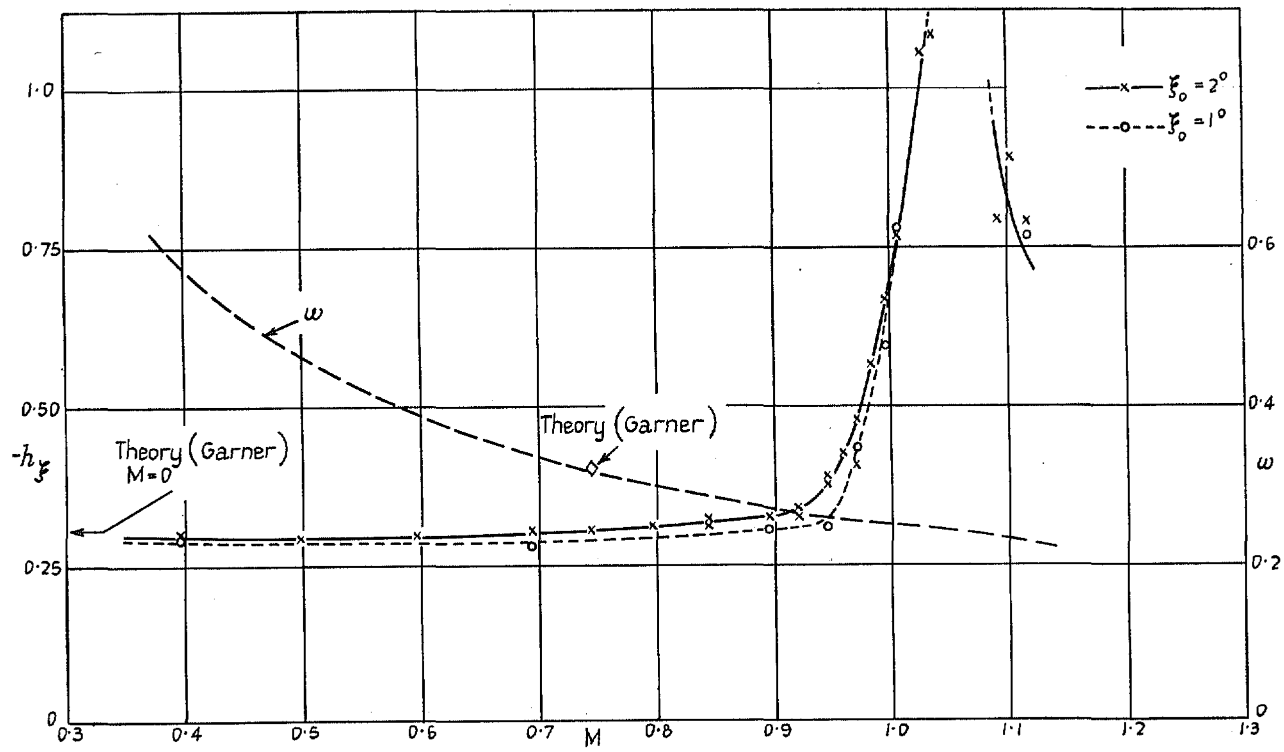

FIG. 11. Variation of $-h_\xi$ and ω with M for $f' = 104$ c.p.s.

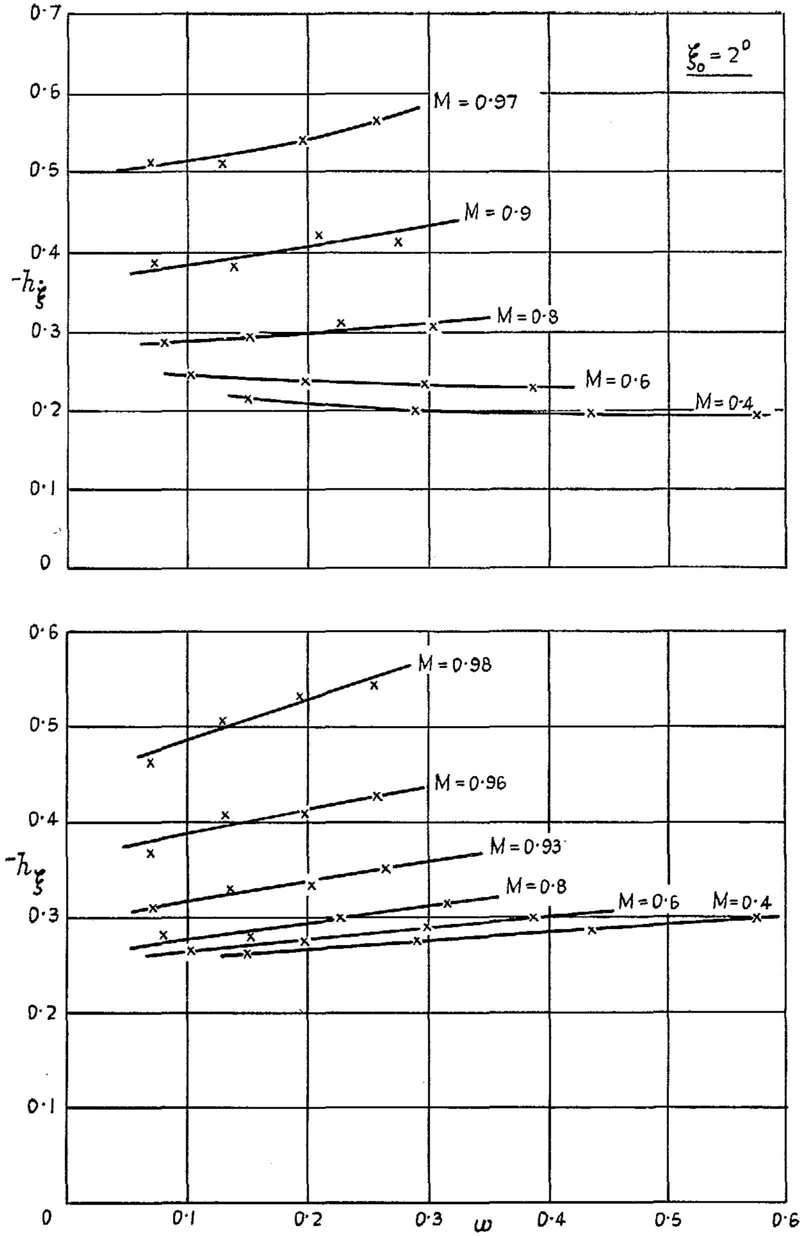

FIG. 12. Variation of $-h^{\dot{\xi}}$ and $-h^{\xi}$ with ω.

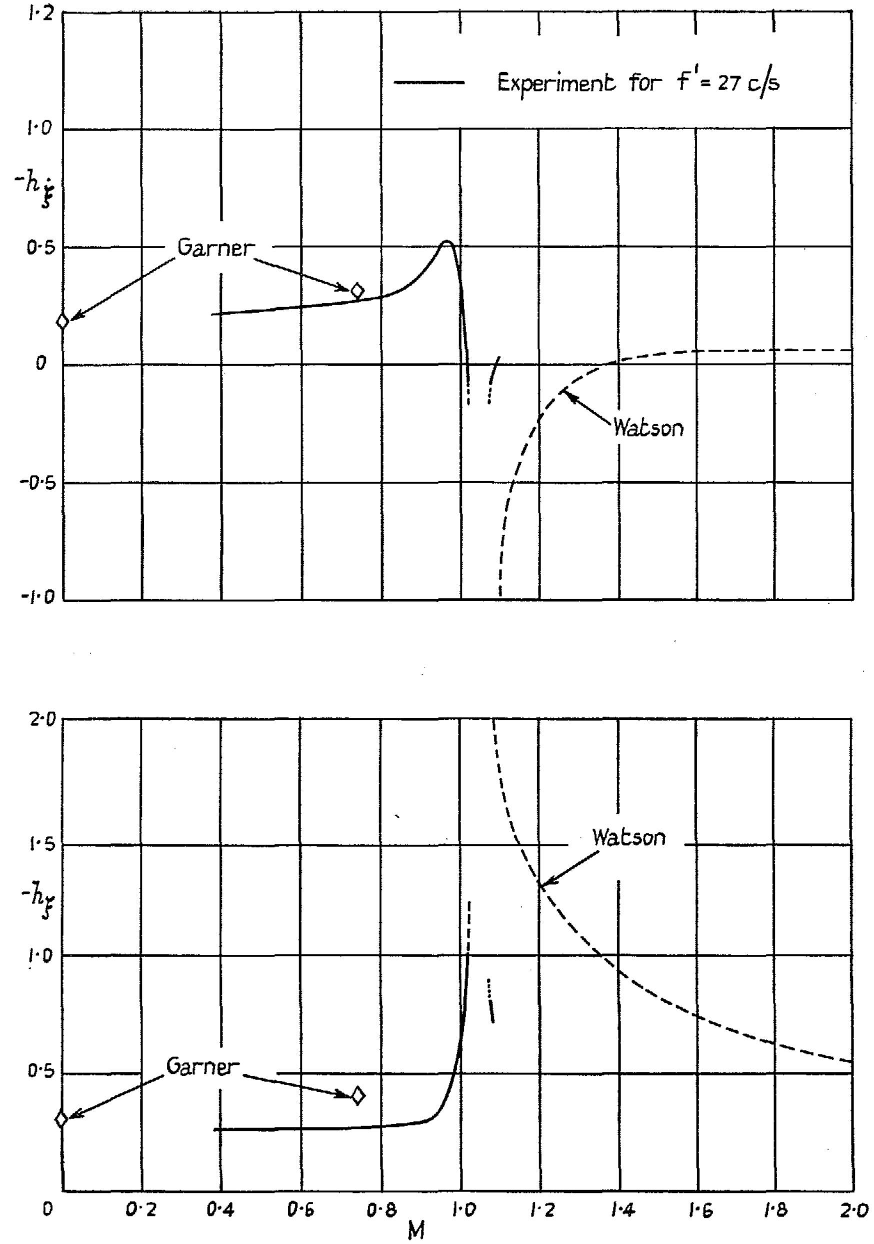

FIG. 13. Comparison of theory with experiment.

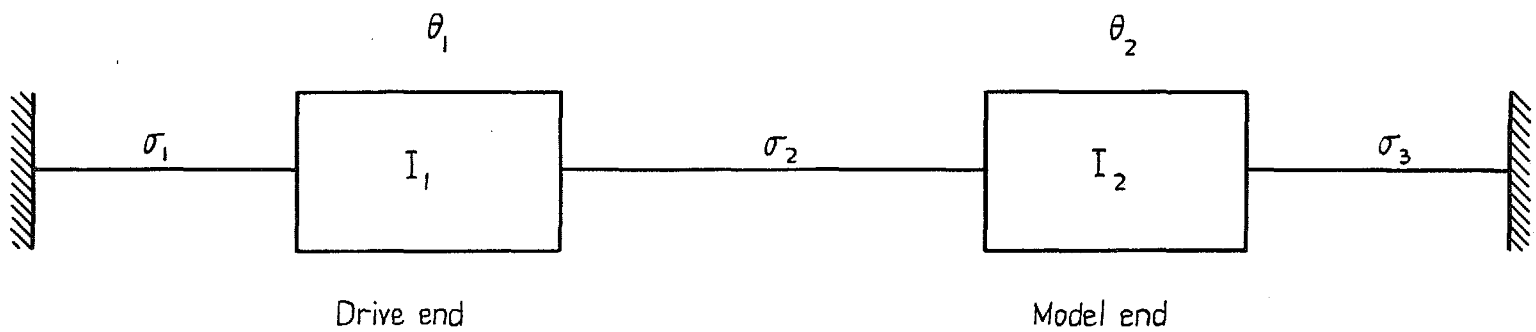

FIG. 14. Theoretical diagram of vibratory system.

(78292) Wt. 3523/8210 K.7 8/60 Hw.

PRINTED IN ENGLAND

Publications of the Aeronautical Research Council

ANNUAL TECHNICAL REPORTS OF THE AERONAUTICAL RESEARCH COUNCIL (BOUND VOLUMES)

1939 Vol. I. Aerodynamics General, Performance, Airscrews, Engines. 50*s.* (52*s.*).
Vol. II. Stability and Control, Flutter and Vibration, Instruments, Structures, Seaplanes, etc. 63*s.* (65*s.*)

1940 Aero and Hydrodynamics, Aerofoils, Airscrews, Engines, Flutter, Icing, Stability and Control, Structures, and a miscellaneous section. 50*s.* (52*s.*)

1941 Aero and Hydrodynamics, Aerofoils, Airscrews, Engines, Flutter, Stability and Control, Structures. 63*s.* (65*s.*)

1942 Vol. I. Aero and Hydrodynamics, Aerofoils, Airscrews, Engines. 75*s.* (77*s.*)
Vol. II. Noise, Parachutes, Stability and Control, Structures, Vibration, Wind Tunnels. 47*s.* 6*d.* (49*s.* 6*d.*)

1943 Vol. I. Aerodynamics, Aerofoils, Airscrews. 80*s.* (82*s.*)
Vol. II. Engines, Flutter, Materials, Parachutes, Performance, Stability and Control, Structures. 90*s.* (92*s.* 9*d.*)

1944 Vol. I. Aero and Hydrodynamics, Aerofoils, Aircraft, Airscrews, Controls. 84*s.* (86*s.* 6*d.*)
Vol. II. Flutter and Vibration, Materials, Miscellaneous, Navigation, Parachutes, Performance, Plates and Panels, Stability, Structures, Test Equipment, Wind Tunnels. 84*s.* (86*s.* 6*d.*)

1945 Vol. I. Aero and Hydrodynamics, Aerofoils. 130*s.* (132*s.* 9*d.*)
Vol. II. Aircraft, Airscrews, Controls. 130*s.* (132*s.* 9*d.*)
Vol. III. Flutter and Vibration, Instruments, Miscellaneous, Parachutes, Plates and Panels, Propulsion. 130*s.* (132*s.* 6*d.*)
Vol. IV. Stability, Structures, Wind Tunnels, Wind Tunnel Technique. 130*s.* (132*s.* 6*d.*)

Annual Reports of the Aeronautical Research Council—

1937 2*s.* (2*s.* 2*d.*) 1938 1*s.* 6*d.* (1*s.* 8*d.*) 1939–48 3*s.* (3*s.* 5*d.*)

Index to all Reports and Memoranda published in the Annual Technical Reports, and separately—

April, 1950 - - - - R. & M. 2600 2*s.* 6*d.* (2*s.* 10*d.*)

Author Index to all Reports and Memoranda of the Aeronautical Research Council—

1909—January, 1954 R. & M. No. 2570 15*s.* (15*s.* 8*d.*)

Indexes to the Technical Reports of the Aeronautical Research Council—

December 1, 1936—June 30, 1939	R. & M. No. 1850	1*s.* 3*d.* (1*s.* 5*d.*)
July 1, 1939—June 30, 1945	R. & M. No. 1950	1*s.* (1*s.* 2*d.*)
July 1, 1945—June 30, 1946	R. & M. No. 2050	1*s.* (1*s.* 2*d.*)
July 1, 1946—December 31, 1946	R. & M. No. 2150	1*s.* 3*d.* (1*s.* 5*d.*)
January 1, 1947—June 30, 1947	R. & M. No. 2250	1*s.* 3*d.* (1*s.* 5*d.*)

Published Reports and Memoranda of the Aeronautical Research Council—

Between Nos. 2251–2349	R. & M. No. 2350	1*s.* 9*d.* (1*s.* 11*d.*)
Between Nos. 2351–2449	R. & M. No. 2450	2*s.* (2*s.* 2*d.*)
Between Nos. 2451–2549	R. & M. No. 2550	2*s.* 6*d.* (2*s.* 10*d.*)
Between Nos. 2551–2649	R. & M. No. 2650	2*s.* 6*d.* (2*s.* 10*d.*)
Between Nos. 2651–2749	R. & M. No. 2750	2*s.* 6*d.* (2*s.* 10*d.*)

Prices in brackets include postage

HER MAJESTY'S STATIONERY OFFICE

York House, Kingsway, London W.C.2; 423 Oxford Street, London W.1; 13a Castle Street, Edinburgh 2; 39 King Street, Manchester 2; 2 Edmund Street, Birmingham 3; 109 St. Mary Street, Cardiff; Tower Lane, Bristol 1; 80 Chichester Street, Belfast, *or through any bookseller.*

S.O. Code No. 23-3163

R. & M. No. 3163